Video-rate imaging of sub-10 nm plasmonic nanoparticles in cellular medium free of background scattering

He Gao, [a] Pei Wu,[a] Pei Song,[a] Bin Kang,[a] Jing-Juan Xu*[a] and Hong-Yuan Chen[a]*

[a] State Key Laboratory of Analytical Chemistry for Life Science and Collaborative

Innovation Center of Chemistry for Life Sciences, School of Chemistry and Chemical

Engineering, Nanjing University, Nanjing 210023, China.

*Correspondence and requests for materials should be addressed to B.K.

(binkang@nju.edu.cn), J.-J.X. (xujj@nju.edu.cn)

CONTENT

Supplementary Note 1: Supplementary Text and Figures

1.1   Theory model of imaging

1.2   Optical system configuration and data analysis

1.3   Simulation of imaging methods

Supplementary Note 2: Relevant data and analysis

2.1   Elimination of strong scattering background by AMSM method

2.2   Data processing process

2.3   In vitro imaging of small size nanoparticles

2.4   Imaging and data analysis of small-size nanoparticles in cell

2.5   Plasmonic nanoparticles characterization

Supplementary Note 3: Supplementary Videos

Supplementary Note 1: Supplementary Text and Figures

1.1 Theory model of imaging

1.1.1 Laser heating of nanoparticles

The heating time is 5-7 ns, and the heat that is diffused to the surrounding medium during heating is ignored. The gold is small enough, so when it is heated, the entire gold temperature is considered consisted. (OMT model).[1-3] During the heating process, the gold and the external environment can be regarded as a continuum. At the same time, the heating frequency of 20 Hz can not cause the temperature rise of the whole environment. After heating, only the temperature of gold nanoparticles and the local thermal field around the particles change.

The 532 nm pulse laser, which matches its maximum absorbance band, is used to heat gold nanoparticles due to the surface plasmon resonance effect.

The heating process could be written as

$$Q_{Au} = \frac{\sigma_{abs} \cdot P}{A_{pump}} = \rho_{Au} c_{Au} V_{Au} \Delta T_{Au}$$

Where P is the pulse energy of the heating laser, σ_{abs} is a constant related to absorption cross section of nanoparticles, A_{pump} is the effective area of the beam cross section, Q_{Au} is the absorbed energy of a single gold nanoparticle, ρ_{Au} is the density of gold (19320 kg·m^{-3}), c_{Au} is the specific heat capacity of gold (129 J·kg^{-1}·K^{-1}), V_{Au} is the volume of the Au nanoparticle, ΔT_{Au} is the temperature difference between the gold nanoparticle and the surrounding medium after being heated by the pulse laser.

1.1.2 Optical signal

Unlike traditional photothermal techniques in which a stable thermal field is formed around a nanoparticle, the thermal field in our system is non-equilibrium and changing with time. The temperature change of the external medium causes the change of refractive index of the medium. Generally, the refractive index of the liquid becomes smaller as the temperature increases, thus a nano-scale thermal lens is formed around the gold nanoparticles.[4] Since time-

varying thermal field is difficult to describe with specific equations, we make a reasonable approximation of the system.

The detected signal $\Phi=(I_{ON} - I_{OFF})/I_{OFF}$, where I_{ON} is the scattered light intensity detected immediately after the gold nanoparticle heating process, I_{OFF} is the intensity of the scattered light detected after the gold nanoparticles are completely cooled. $\Delta I= I_{ON}-I_{OFF}$ arrives from the change of refractive index (n) of the liquid surrounding gold nanoparticle. We could approximate the actual change value $n(r, t)_m$ by using the average of the refractive index changes

$$\bar{n}(t)_m = \frac{\int n(t,r)dV}{\int dV}.$$

This average includes two approximations, first of all the average of the refractive indices of the media. At the same time, the thermal field changes with time. Once the laser energy and the time width of detection are unchanged, the thermal field during the detection process $\bar{n}(t)_m$ could be expressed as:

$$\bar{n} = \frac{\iint n(r,t)drdt}{\int dv}$$

The signal is acquired immediately after the heating step. We approximate that the temperature of plasma layer does not change during the acquisition process.

$\bar{n}$ can be approximated as

$$\bar{n} = \frac{\int n(r)dr}{\int dv}$$

Where $\int dv$ refers to the physical volume of the plasma layer.

The expression of refractive index in the thermal field can be written as

$$n(r) = n_0 + \Delta n(r)$$

So the change in refractive index can be written as[5-7]

$$\Delta n = \bar{n} - n_0$$

Where n_0 is the refractive index of the surrounding medium without laser heating. The

photothermal signal we detected could be expressed as

$$\Phi = \frac{I_{ON} - I_{OFF}}{I_{OFF}} \propto \Delta n$$

Bring the above expression about the refractive index into the photothermal signal

$$\Phi = A \int \Delta n(r)dr$$

In above equation, A is a constant independent of the refractive index. The refractive index of the medium has the following relationship with the temperature of the medium.

$$\Delta n = \Delta T \frac{\partial n}{\partial T}$$

.

$\frac{\partial n}{\partial T}$ is the variation of the refractive index with temperature (typically ： $-10^{-4}\,K^{-1}$).

The photothermal signal can be further expressed as

$$\Phi = A \int \Delta T_{(r)} \frac{\partial n}{\partial T} dr$$

As discussed above, the temperature of the gold and surrounding media are continuum, and the plasma layer thickness is relatively small for the entire heat dissipation range, and the plasma layer temperature is considered to be fixed within the measurement gate width. Therefore, we can correlate the temperature of the medium in the plasma layer with the temperature of the gold nanoparticle.

$$\Delta \overline{T} = B \cdot \Delta T(0)_{Au}$$

$$Q_{Au} = \frac{\sigma_{abs}.P}{A_{pump}} = \rho_{Au} c_{Au} V_{Au} \Delta T(0)_{Au}$$

Further expression of the photothermal signal is represented as

$$\Phi = C \frac{\partial n}{\partial T} \frac{P\sigma_{abs}}{\rho_{Au} c_{Au} V_{Au}}$$

The scattering cross section and volume of the gold nanoparticle are both proportional to the cube of the radius of the gold nanoparticle.

$$\sigma_{abs} \propto r_{Au}{}^{3} \qquad V_{Au} \propto r_{Au}{}^{3}$$

So the signal can eventually be expressed as

5

$$\Phi = C \frac{\partial n}{\partial T} \frac{P}{\rho_{Au} c_{Au}}$$

According to the formula, the signal can be related to the refractive index of the medium, the laser intensity, the basic physical properties of the medium and the gold nanoparticles. Among them, the signal is proportional to the laser intensity but inversely proportional to the refractive index of the medium. Most importantly, it can be concluded from the formula that the intensity of the signal is independent of the radius of the gold nanoparticles, which theoretically demonstrates the possibility of imaging sub-10 nm particles.

1.2 Optical system configuration and data analysis
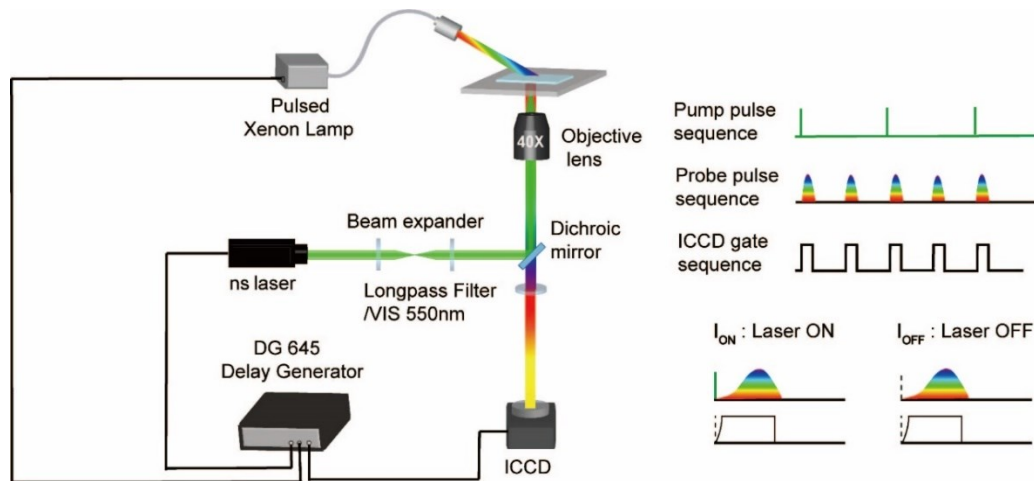
Fig. S1 Schematic diagram of self-built absorption modulating scattering microscopy (AMSM) device and sequence of detection process

We use pump-probe technology to complete the imaging with our homemade transient imaging microscope. A nanosecond pulsed laser (20 Hz, 5~7 ns) was used as the pumping beam, and the laser beam was expanded to a spot size of about 200 μm before it was focused on the sample platform. A pulsed white xenon lamp is used as the detection light source to detect the scattering light changes of gold nanoparticles during the process. The spot size of the detection light source on the sample plane is about 1 mm, which can cover all gold nanoparticles in the whole laser-heated area. Subsequently, the scattered light of gold nanoparticles was collected and imaged by ICCD through a 40X objective lens. In this process, to prevent the heating laser

from leaking into ICCD, a long pass 540 filter is added before ICCD to filter out the laser that may enter.

The time zero of the system is the start time of the laser heating, and the pulsed xenon lamp and ICCD gate time are controlled by a delay generator (DG 645) with a transistor-transistor logic (TTL) triggering signal with a rising edge of 2 ns. The TTL signal triggers the opening of the pulsed xenon lamp and the ICCD detector gate. Since the 6 μs pulse xenon lamp start-up time and the 19 ns ICCD gate trigger time are not completely synchronized, we set the ICCD gate width to 10 μs to collect the high-intensity portion of the pulsed xenon lamp with a duration of 6 μs.

In a complete probing process, the gold nanoparticles are first heated by the laser for 5-7 ns. After the gold nanoparticles are heated, the system is triggered by a TTL signal to capture the scattered signal (I_{ON}) of the heated gold nanoparticles. The gold nanoparticles are then naturally cooled to transfer heat to the surrounding medium. After the gold nanoparticles are completely cooled, the intensity of the scattered light is measured, which is called I_{OFF}. Therefore, in a completed detection process, the pump source is used for one single heating and the detection source captures the scattered light in two states. The frequency of the heating laser was 20 Hz, and the frequencies of pulsed xenon lamp and ICCD were modulated to 40 Hz. For this intermediate detection, the gold nanoparticles can be completely cooled. The system performs a set of I_{ON} and I_{OFF} detections at a frequency of 20 Hz. Subsequently, we subtract each set of detection images to obtain the desired photothermal signal map.

1.3   Simulation of spectra
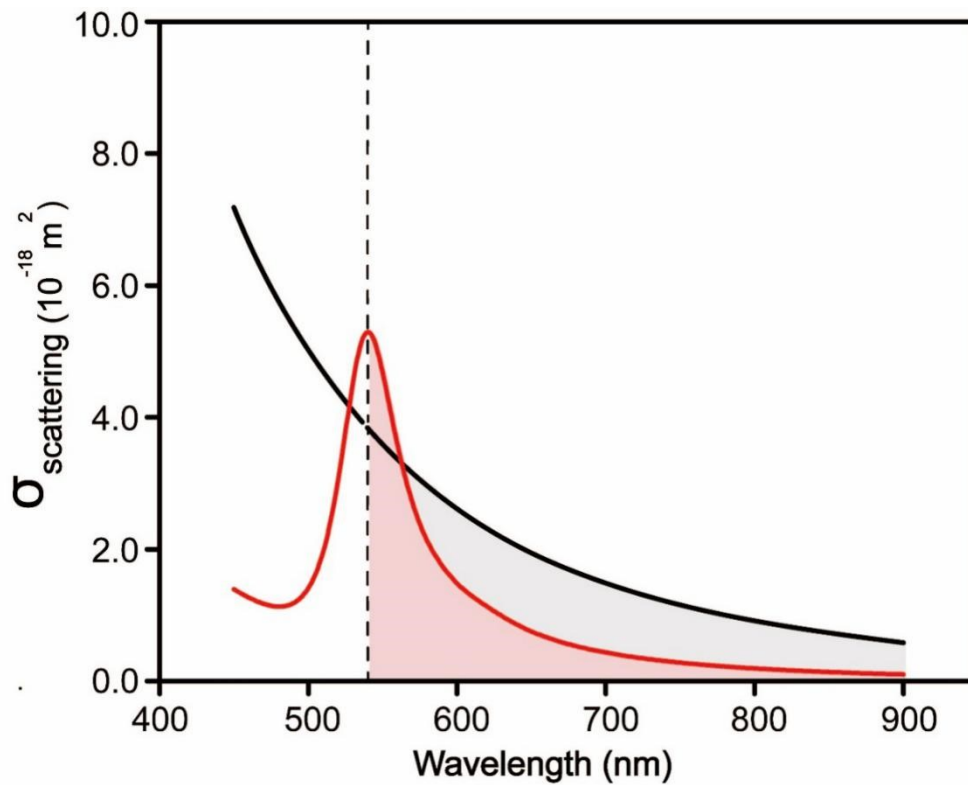
Fig. S2 FDTD simulation of the scattering spectra of different particles (red line: 20 nm gold nanoparticle; black line: 100 nm lipid particle)

In the experiment, gold nanoparticles with special resonance scattering were efficiently extracted in a strong scattering background. We added a long pass 540 filter behind the objective to aid in signal extraction. To illustrate that our modification is more conducive to signal extraction, we use the finite-difference time domain (FDTD) method to simulate the scattering of different particles in cells under different conditions. The refractive index of the intracellular matrix is usually distributed in the range of 1.35-1.37. In the simulation, we use 1.37 as the refractive index of the cells. The highly dispersed organelles in the cells are encapsulated by a phospholipid molecular membrane with a refractive index distribution ranging from 1.38 to 1.47. Therefore, we chose phospholipid spheres with a refractive index of 1.42 as mock objects to represent strongly dispersed organelle particles in cells. We used FDTD to simulate the scattering spectra of a 20 nm gold nanoparticle and a 100 nm lipid particle, respectively. According to the simulation, the scattering intensity of the lipid particles are larger than that of gold nanoparticle, and thus the scattered light of the gold nanoparticles is submerged in the strongly scattering signal from the cell background particles. But when we

added the long pass 540 filter to the system, we only collected light with wavelength longer than 540 nm. As indicated by the shaded portion in figure S2, the red region represents the portion of scattered light from the gold nanoparticle, and the gray region is the portion from lipid particle. After the addition of the 540 long pass filter, the scattering light in the wavelength range shorter than 540 nm from cellular scattering components like liposome is filtered out, and the intensity of the remaining portion is lower than that of gold nanoparticle (according to the area integral of corresponding scattering cross section).This modification allows us to reduce the strong and wide background scattering effects within the cell, thereby facilitating the capture of the desired signal.

Supplementary Note 2: Supplementary data and analysis

2.1   Elimination of strong scattering background by AMSM method
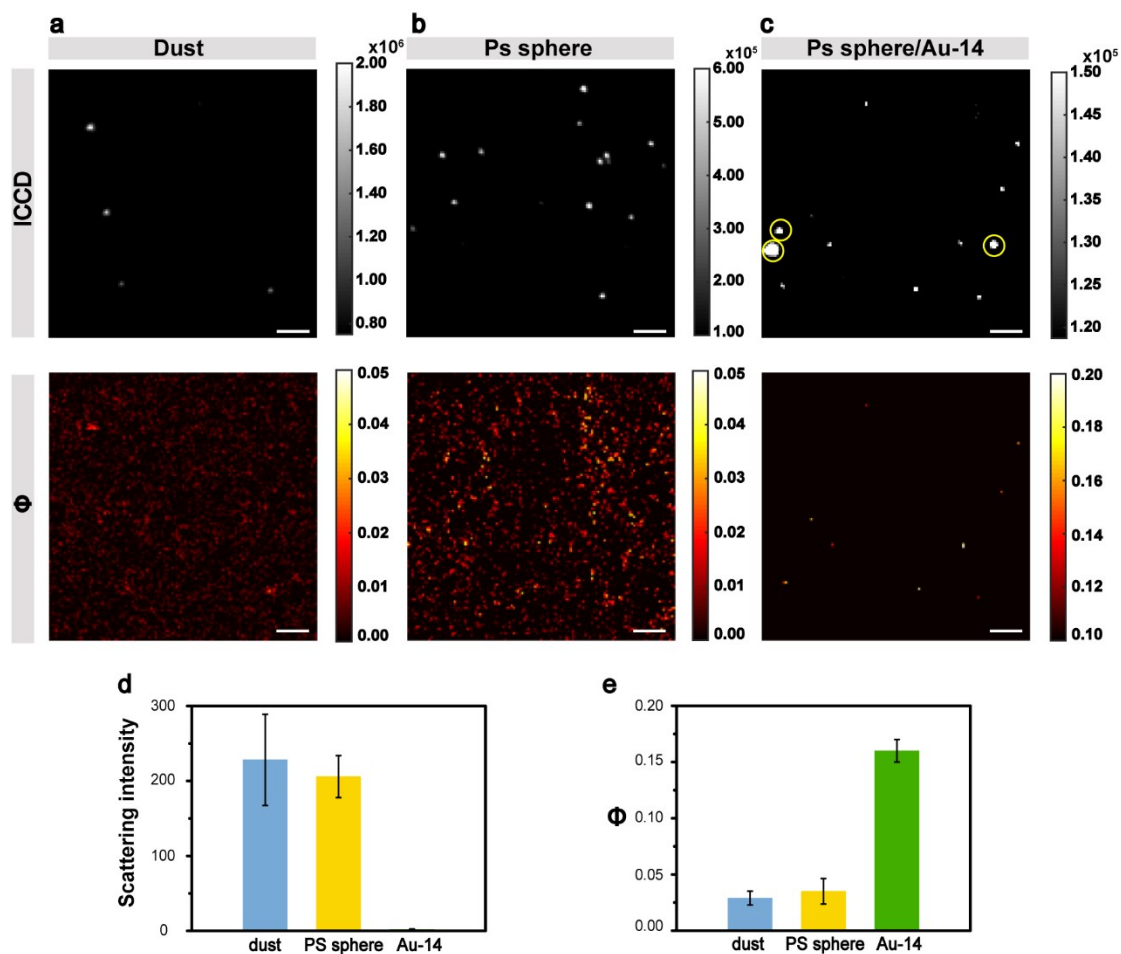
Fig. S3 Imaging analysis of different particles (a) ICCD image and Φ signal image of dust particles in glass substrate. (b) ICCD image and Φ signal image of polystyrene spheres in glass

substrate. (c) ICCD image and Φ signal image of mixture of polystyrene spheres and 14 nm gold nanoparticles in glass substrate. (scale bars: 10 μm. Yellow circles: polystyrene spheres). (d) Scattered light intensity and (e) Φ signal intensity of different particles.

For future applications of our method for single-particle intracellular imaging, the effects of intracellular background and other particle scattering on photothermal images must be considered. In vitro experiments, there are also some strong scattering materials, such as the dust adsorbed on the positive glass plate will affect the ordinary dark field imaging. Dust and 300 nm polystyrene spheres have strong scattering properties that cause background interference in the imaging process. Therefore, three planking experiments were performed using dust, polystyrene spheres (ps spheres) and a mixture of polystyrene spheres and 14 nm gold nanoparticles (Fig. S3 a-c). Figure S7-a records the scattered light of randomly adhered dust on a glass plate. Due to the varied size and shape of the dust, the scattered light intensity of the particles varies greatly, and the intensity is mostly greater than $1*10^6$. However, in figure S7-b, the uniformity of the size of the polystyrene spheres results in a large intensity and a small distribution range of the scattered light. But, the photothermal signals of the two particles are very weak, with an average of 0.029 and 0.035, respectively, which can be identified as noise. This shows that our method is insensitive to scatterers with non-specific absorption. In the mixture plating experiment of figure S3-c, the signal of polystyrene sphere circled in yellow must overexposure greatly to allow the detector to reach the 14 nm gold nanoparticle signal. However, in the Φ signal map, 14 nm gold nanoparticles can be found one by one corresponding to dark field images, while polystyrene spheres with strong scattering can be removed as noise due to extremely low signal. The scattered light and Φ signal intensity of the particles in the three images are further counted to obtain figure S7-d, e. Even if the difference in the scattered signal reaches about 2,500, the signal value of the particles in the Φ signal is 4.5 times or more of the other two kinds of particles. It is proved that the method is only responsive to objects that specifically absorbed light, and the background scattering cannot be converted into a strong noise signal in the Φ signal map. If further tested in a biological sample, the background signal can also be ignored as noise in the Φ signal map.

2.2 Data processing process
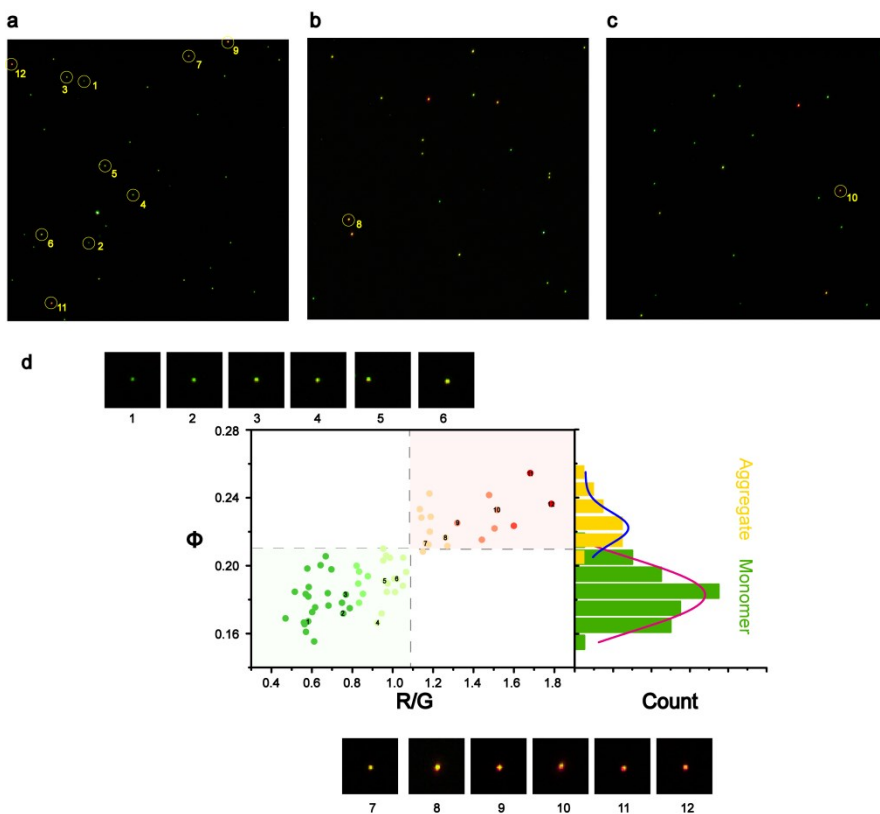
Fig. S4 Actual data presentation in Fig.2d

Because the data in figure 2d comes from multiple sets of experiments. We selected some particles of different states, monomers and aggregates, to illustrate our method of data extraction. We show the positions of some points in Fig. S4 (d) in the original data. Here, particles No. 1-12 are selected. According to the dark field image, we can see that the R/G value corresponding to the No.1-6 is lower than 1.1. According to the scattering characteristics of gold nanoparticles, these particles are monomer 80 nm gold nanoparticles. At the same time, the AMSM signal corresponding to these monomer particles is less than 0.21. In the experiment, most of the AMSM signals obtained from the 80nm gold nanoparticles determined by R/G value were distributed in the lower left of the scatter diagram. However, in the dark field, particles 7-12 with relatively large R/G value are identified as aggregates. Those aggregated nanoparticles have larger AMSM signal than monmomer, thereby localized at the upper right region of the scatter diagram.
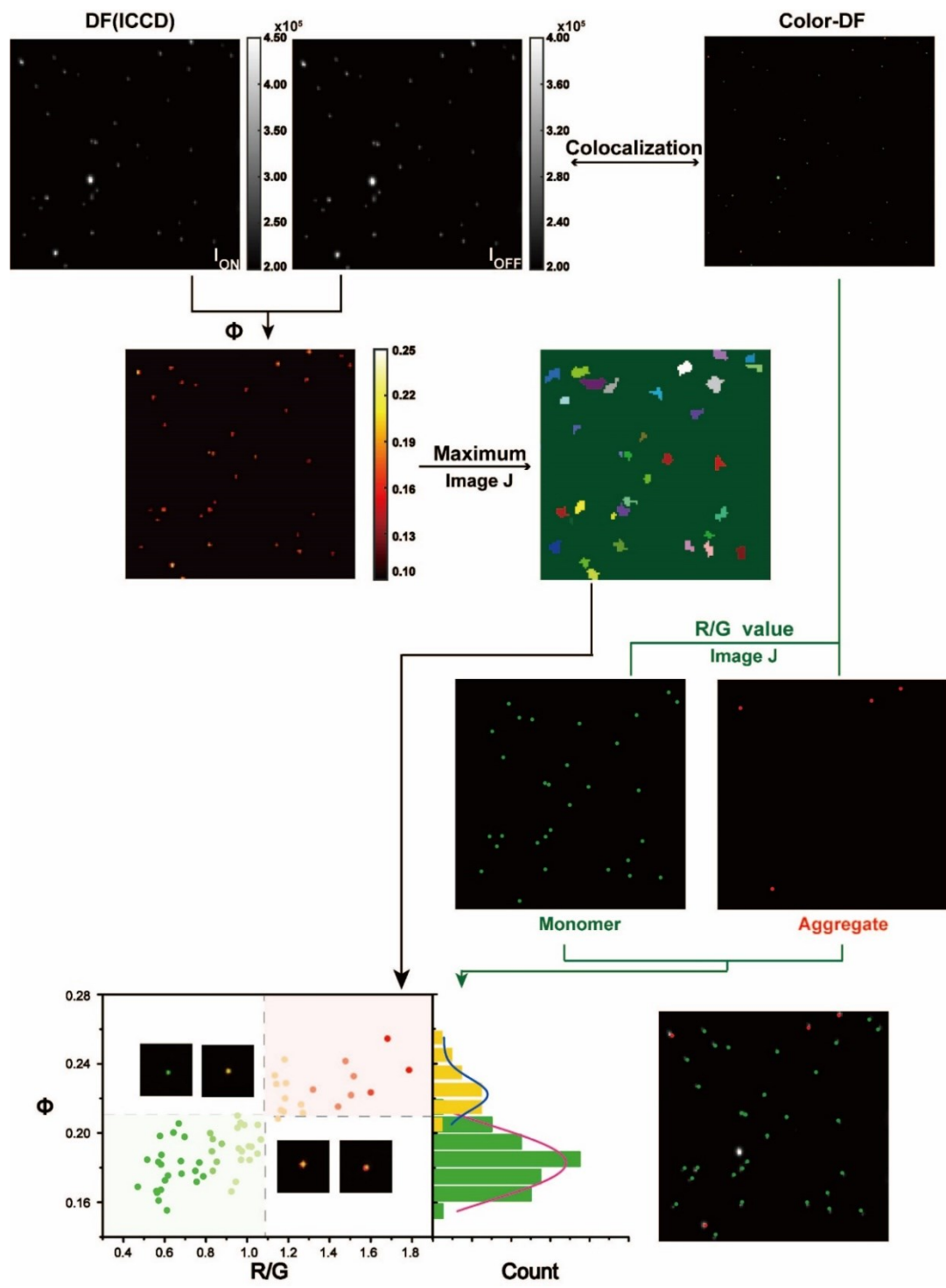
Fig. S5 Process for large size gold nanoparticle.

In the imaging of large-sized gold nanoparticles, a conventional color dark field imaging is carried in the system to complete the co-localization experiment. First, a series of I_{ON} and I_{OFF} are taken for the selected area to collect ICCD dark field data. In the end, the traditional dark field imaging is performed on the same region of interest. For the previously acquired ICCD dark field image, I_{ON} and I_{OFF} are subtracted to obtain a Φ signal map. Further, ImageJ

12

software extracts the maximum value of the area around each particle in the Φ signal map to obtain the Φ value of each particle. The Image J was used to split the red, green, and blue color channels of color dark field scattering image, then the R/G value were calculated. By the different the R/G ratio, two separate distribution images of the monomer and the aggregate can be obtained on the original color picture. We collect the data after the co-localization experiment and summarize a scatter plot with the abscissa as the R/G value and the ordinate as the Φ value. The right picture is a separate count of the Φ value data for the monomers and aggregates. It can be concluded from the scatter plot that the Φ value can be used to distinguish the monomer and aggregate states of the gold nanoparticles just as the scattered light R/G value do. To further verify the accuracy of the process, the pictures of the monomers and aggregates were superimposed with the dark field pictures taken by ICCD. The position of the photothermal signal coincides with the position of the color CCD particles, proving that the signal is indeed derived from the particles. At the same time, it can be seen that the particle state distinguished by the color CCD coincides with the particle state distinguished by the Φ value, which proves that the absorption modulated scattering imaging successfully completes the state discrimination of the gold nanoparticle at the same time.

2.3 In vitro imaging of small size nanoparticles
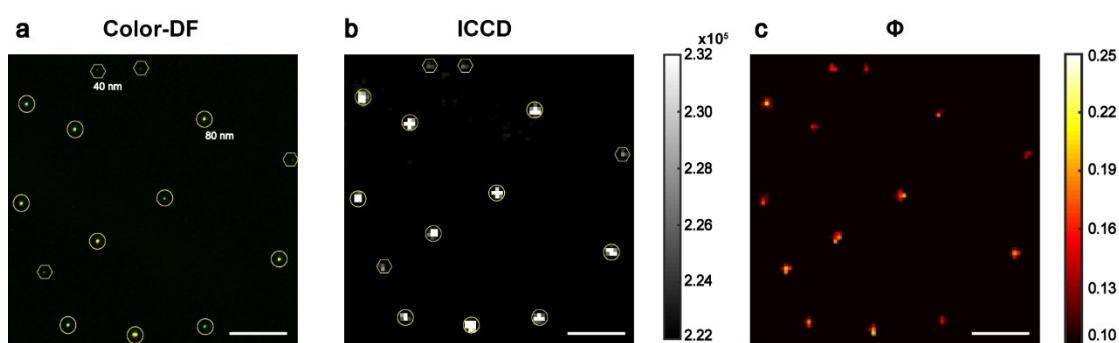
Fig. S6 Colocalization imaging analysis of 80-39 nm gold nanoparticles (a) color dark field image, (b) ICCD image, and (c) Φ signal image of nanoparticles on glass substrate. (scale bars: 10 μm). Yellow circle: 80 nm gold nanoparticles. Yellow hexagon: 39 nm gold nanoparticles.
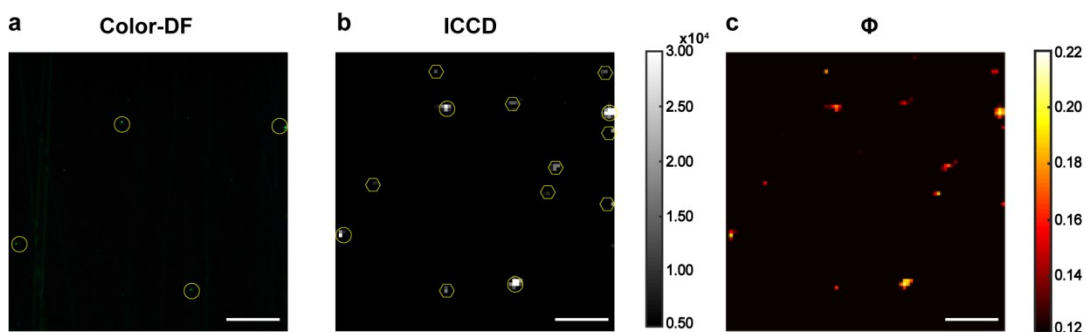
Fig. S7 Colocalization imaging analysis of 39-14 nm gold nanoparticles (a) color dark field image, (b) ICCD image, and (c) Φ signal image of nanoparticles on glass substrate. (scale bars: 10 μm). Yellow circle: 39 nm gold nanoparticles. Yellow hexagon: 14 nm gold nanoparticles.
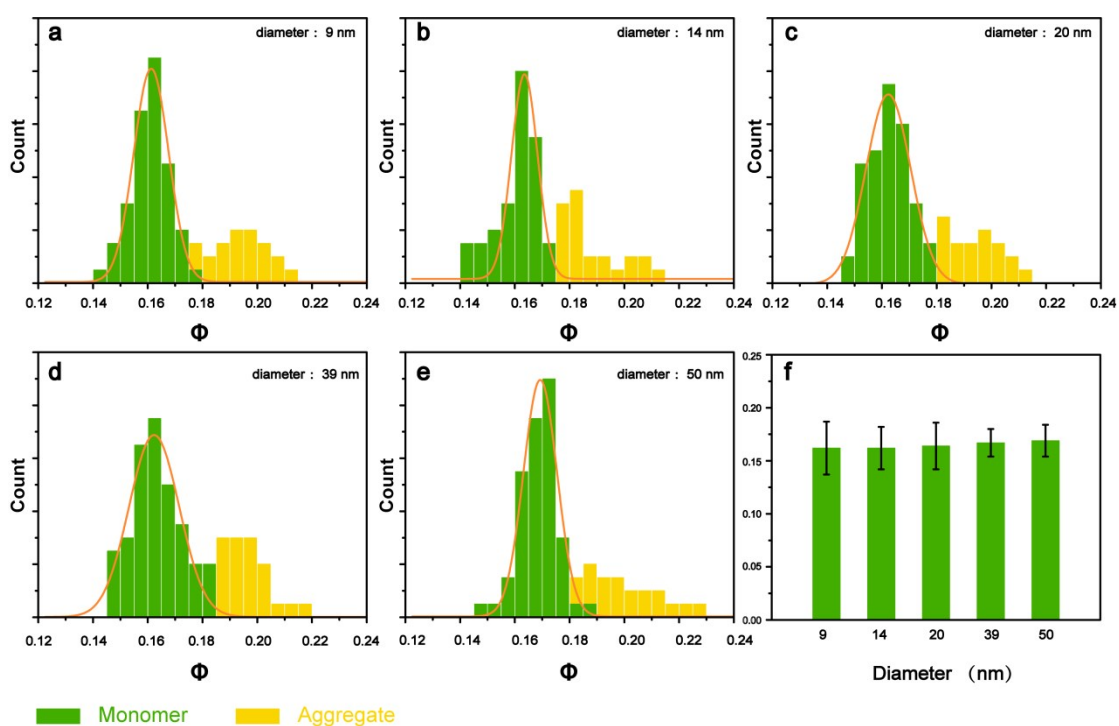
Fig. S8 Φ distribution histogram of sizes gold nanoparticles with different sizes: Φ distribution histogram of (a) 9 nm, (b) 14 nm, (c) 20 nm gold nanoparticle, (d) 39 nm gold nanoparticle and (e) 50 nm gold nanoparticle. (f) Φ signal value of gold nanoparticles with different sizes.

The co-localization imaging of 80-39, 39-14nm gold nanoparticles shows that our AMSM method enables the imaging of very small gold nanoparticles. And the AMSM imaging method is independent of the particle radius. Further, we performed in vitro AMSM imaging of gold nanoparticles with radius of 50, 39, 20, 14, 9 nm (**Fig. S8** a-e). According to data statistics, the distribution of AMSM signals of these gold nanoparticles is similar to that of larger gold

nanoparticles. A large number of monomer particle signals are distributed in a Gaussian distribution between 0.14 and 0.18. The data corresponds to the green bar chart and the orange-red fitting curve. However, particles distributed in the yellow histogram are considered as aggregates and have a larger AMSM signal value. **Fig. S8**-f shows the AMSM signal of gold nanoparticles of 50, 39, 20, 14 and 9 nm. The change in signal intensity is about 8% which could be considered pretty much the same if compared with the dramatically drop in particle size.

Further explain the experimental results on the glass plate. The actual data of some statistical results are shown in Figure S9. Figure S9 shows the darkfield and AMSM signal diagrams of 9nm, 14nm, 20nm, 39nm, and 80nm gold nanoparticles. Analyzing the darkfield image shows that as the particle size increases, the darkfield scattering of the particles increases. Extract more experimental data, and obtain the fitting relationship between the scattering intensity and the particle size in Figure S10. Figure S9 also shows the AMSM signal map corresponding to the darkfield image. It can be seen that as the particle size increases, the intensity of the signal value has been maintained at a strong level.
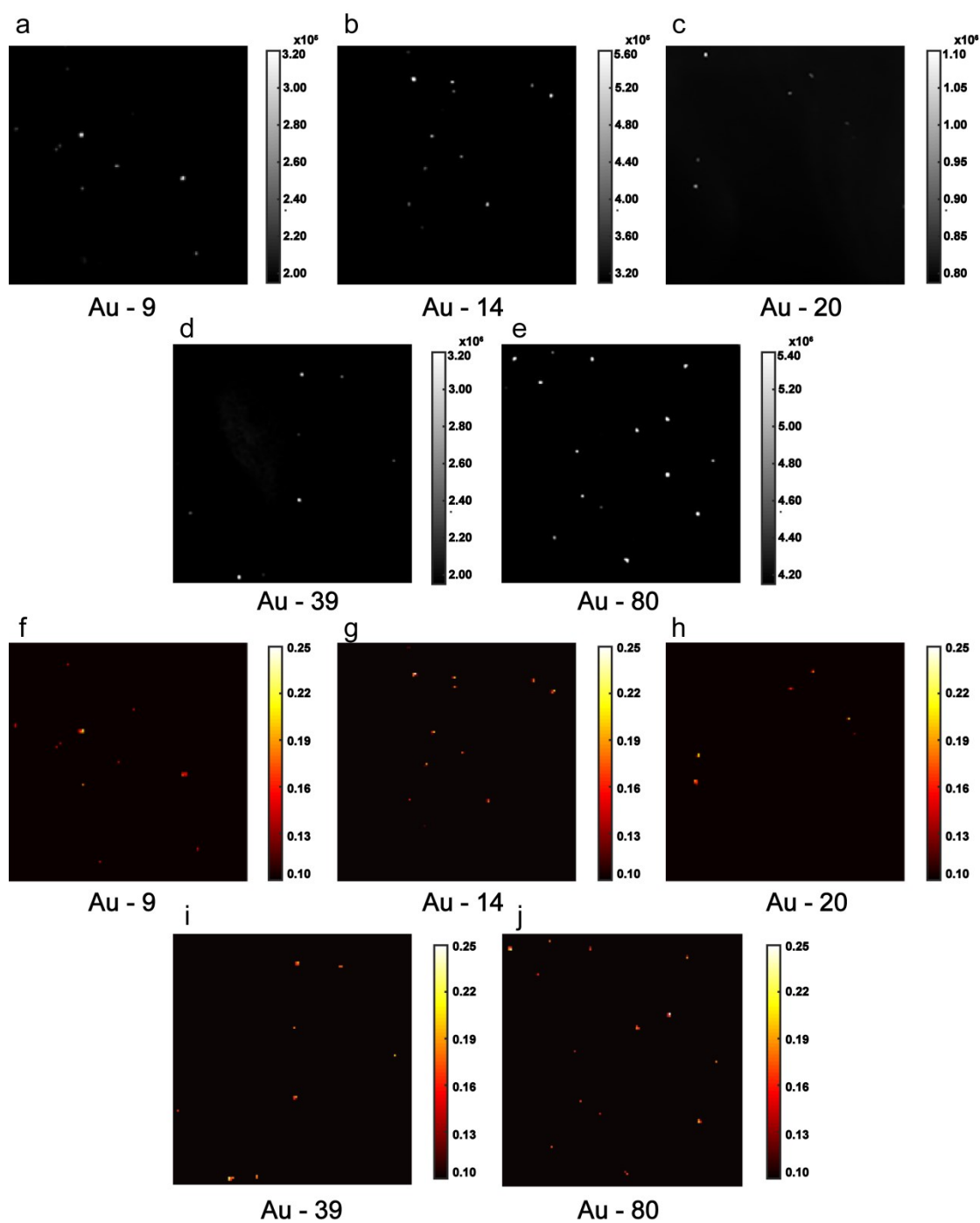
Fig. S9 Imaging of gold nanoparticles of different sizes. (a-e) Dark field scattering image of 9, 14, 20, 39, 80 nm gold nanoparticles captured by ICCD, (f-j) AMSM Φ signal images of 9, 14, 20, 39, 80 nm gold nanoparticles.
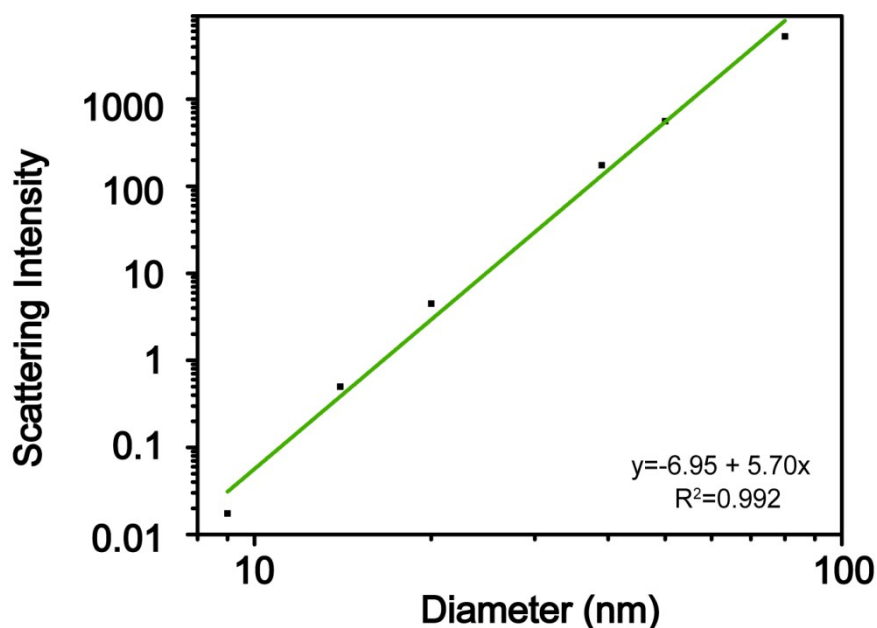
Fig. S10 Logarithm of scattering light intensity versus particle size.

The different particle sizes and the corresponding scattering intensity collected on our glass plate are fitted after taking the logarithm. The text shows exponential fitting, the value 5.73 is very close to the theoretical value 6. After the logarithmic fitting, the obtained slope is 5.70, which is also very close to the theoretical value. It shows that what we have collected is indeed the scattered light intensity of single gold nanoparticles.
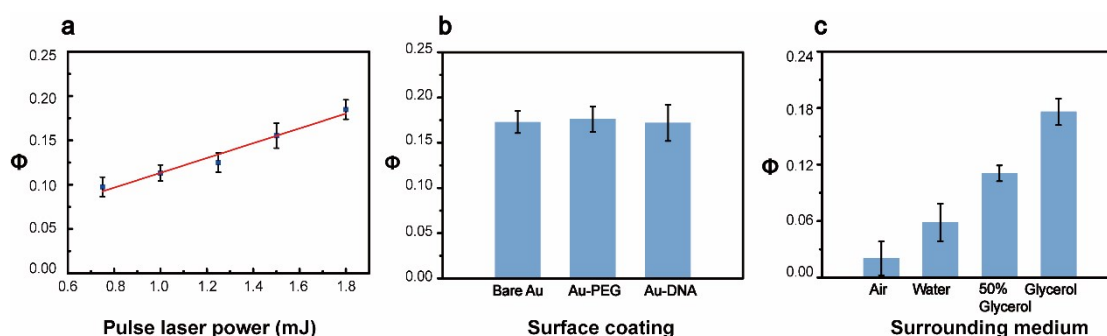
Fig. S11 Influence of measurement conditions on the result of Φ signal value (a-c) Measured Φ signal under different pump energies (a), surface conjugations (b), and surrounding medium (c).

The intensity of the heated laser, the nature of the gold nanoparticles and the refractive index of the surrounding medium can all affect the signal intensity. For the heating laser intensity, as the power increases, the Φ signal value increases linearly. As shown in figure S9-a, as the laser intensity increasing from 0.75 to 1.8 mJ, the Φ signal intensity of the 80 nm gold

nanoparticles increases linearly from 0.098 to 0.185. Under different particle radius conditions, the laser intensity of 1.8 mJ can meet the requirement of signal greater than 0.15. In the experiment, in order to make the gold nanoparticles adsorbed on the positive glass slides more conveniently, the surface of the gold nanoparticles was decorated with SH-PEG. Thus，the Zeta potential of bared Au, Au-PEG and Au-DNA are all particles are all negative. The Φ intensity of these three types of particles is basically the same, so the modification has little effect on the signal (Fig. S9-b). In the above formula, there is a negative correlation between signal intensity and refractive index. In the experiment, the Φ signals of 80 nm gold nanoparticles are measured in four media, air, water, 50% glycerol and pure glycerol (Fig. S9-c). Since the specific absorption of gold nanoparticles in air cannot form an effective thermal lens effect, the Φ signal of gold nanoparticles is only 0.02 in the air. In the other three media, a thermal lens effect can be effectively formed around the gold nanoparticle. So as the refractive index of the medium decreases, the Φ signal becomes stronger. Consistent with the conclusions of the formula, the signal is more stable and larger in glycerol with a refractive index of 1.36 compared to water with a refractive index of 1.33.

2.4　Imaging and data analysis of small-size nanoparticles in cell
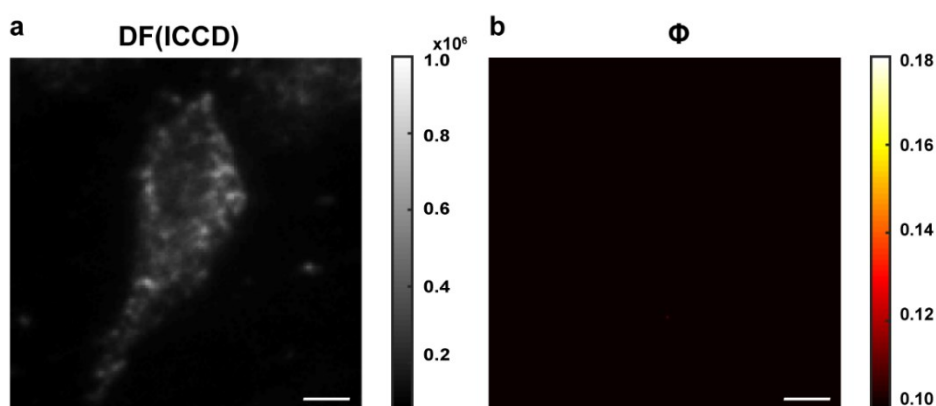
Fig. S12 Imaging of HeLa cells without gold nanoparticles. (scale bars: 10 μm)
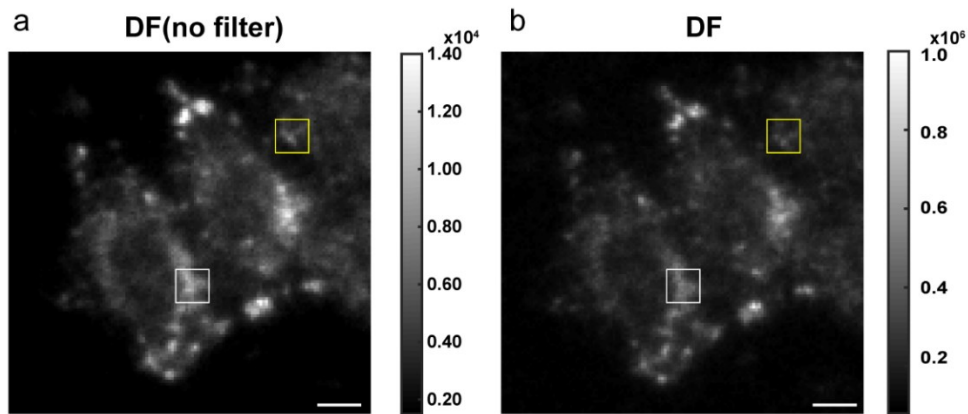
Fig. S13 The change of signal to noise ratio without (a) and with (b) a filter in the system. (scale bars: 10 μm)

In the actual experiment, we verified the improvement of the signal extraction by the addition of the filter. The cells incubated with 20 nm gold nanoparticles were imaged in the presence or absence of filter. In figure S11, (a) is a dark field image without a filter, and (b) is an image with a 540 long pass filter. In the figure, the yellow square region shows the scattering signal from gold nanoparticles. The white square shows scattering signal from cellular component, which is regarded as the background scattering signal from the cell itself. Comparing the yellow and white frames in figure (a), the partial background scattering signal of the cells is stronger than the scattering signal from of gold nanoparticles. However, when the two images (a) and (b) are compared, it can be seen that the quality of cell image is improved after the addition of filter. Specifically, the signal intensity in the white frame is reduced, and the strong scattering is partially filtered out. In the yellow frame, after adding the filter, the particles in the frame are better distinguished. Further, comparing the signal-to-noise ratio, the white-frame signal-to-noise ratio was changed from 3.28 to 3.33, while the yellow frame was increased from 3.97 to 4.63. It is proved that the signal extraction of gold nanoparticles is indeed improved after the addition of the filter.
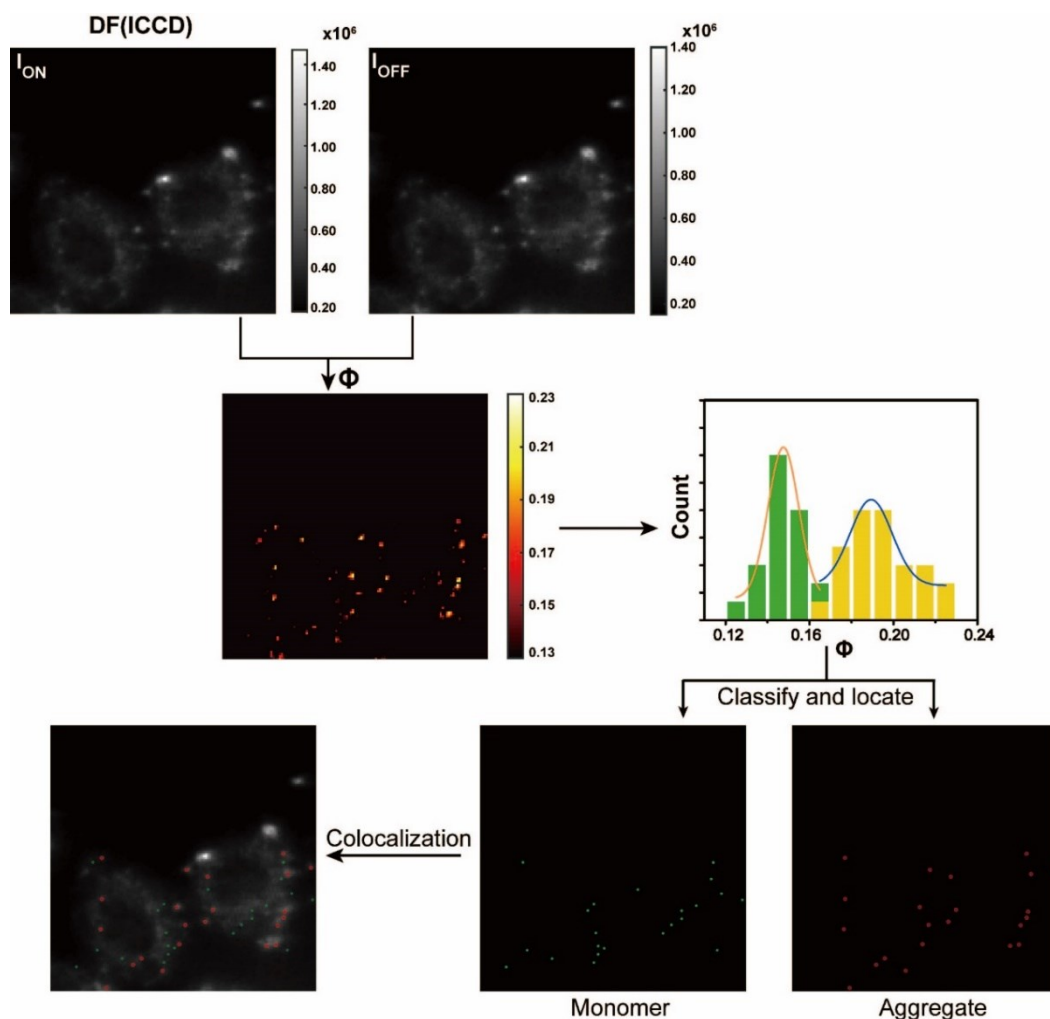
Fig. S14 Imaging process for small size gold nanoparticles.

Since small-sized nanoparticles cannot be imaged with ordinary color CCD darkfield, we only use dark field modulation scattering to image. According to the reasoning of the previous large particle processing, we try to separate the signal intensity of the Φ signal map to see if the particle state can be distinguished. First, the ICCD is used to capture the scattered light of the gold nanoparticles in both the heated and fully cooled states, namely I_{ON} and I_{OFF}. Also, I_{ON} and I_{OFF} are subtracted to obtain a Φ signal map. We extract the Φ value information from the Φ value map and obtain the histogram of the particle signal distribution.[8] In the histogram, there is still a distinction between the two signal intensity of the particles, which is consistent with our previous conclusions. Therefore, we extract the position information behind it based on the value of Φ value again, and plot the position into the image to obtain a separate image of the monomer and the aggregate. The position of the monomers and aggregates is clearly marked

by the overlap of the monomers and aggregates as well as the original dark field ICCD image. The small-sized particles were successfully imaged by the absorption modulated darkfield scattering method.
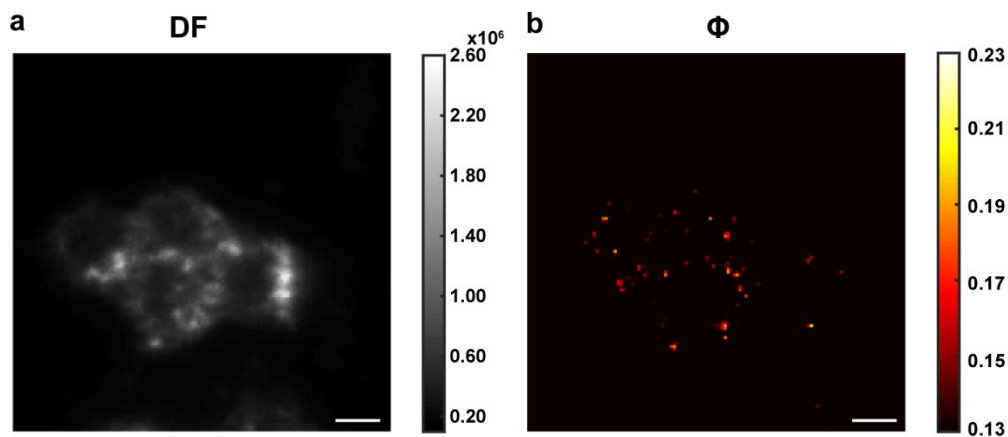
Fig. S15 Imaging of 14 nm gold nanoparticles within MCF-7 cells. (scale bars: 10 μm)

2.5 Plasmonic nanoparticles characterization
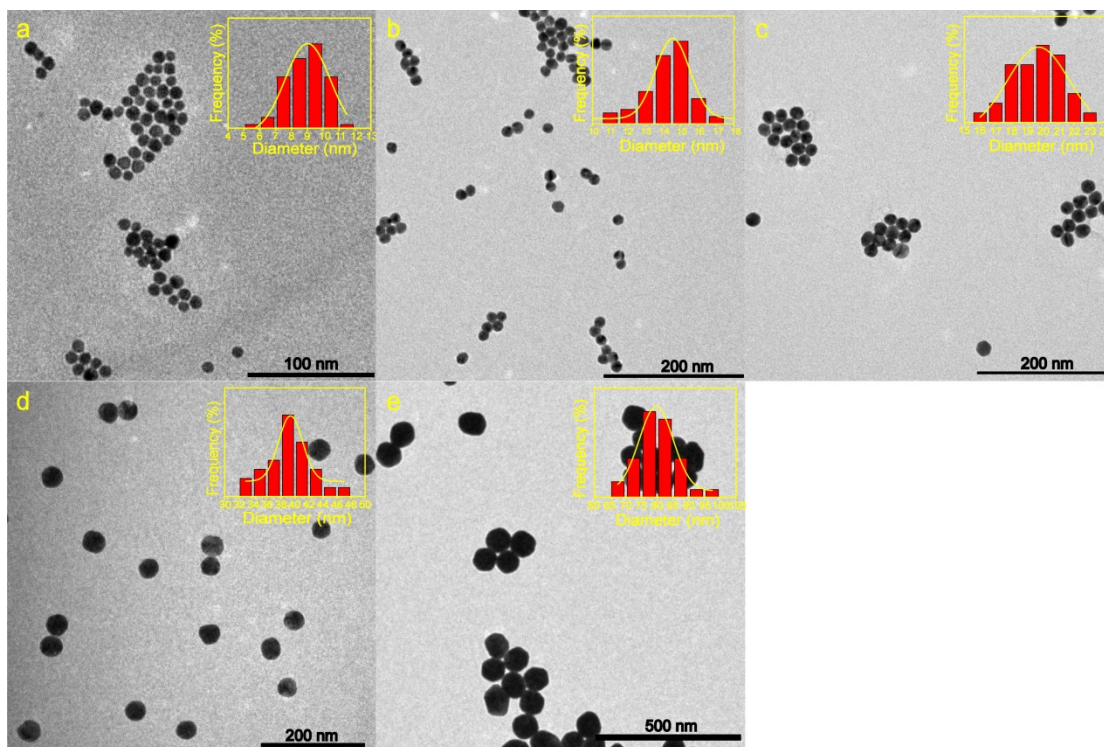
Fig. S16 TEM images of the gold nanoparticles. Mean particle sizes are about (a) 9±2.8 nm ,(b) 14±1.9 nm (c) 20±3.9 nm, (d) 39±3.4 nm and (e) 80±5.4 nm.
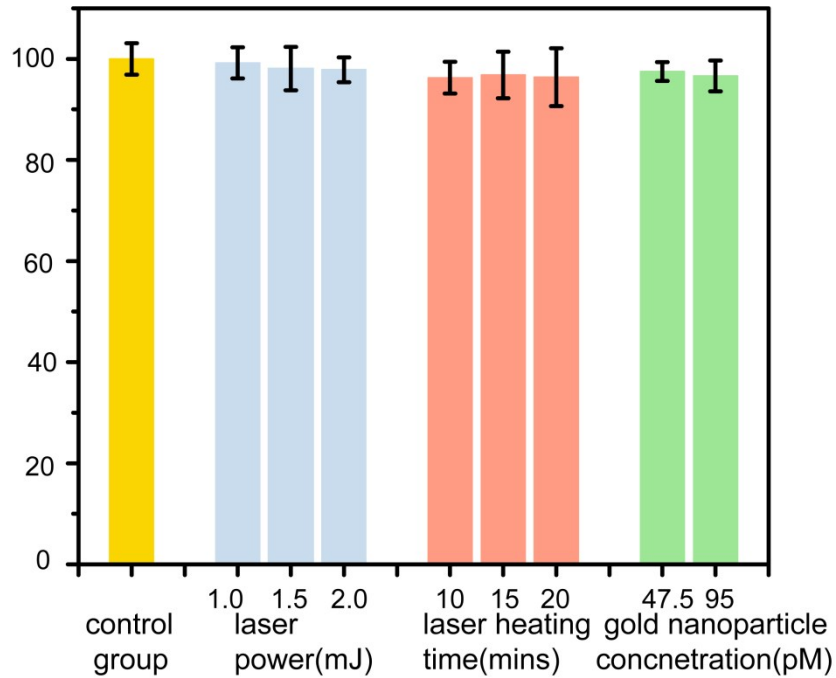
Fig. S17 The cell viability under the different experimental conditions.

Cell viability was determined by MTT (3-(4,5-Dimethylthiazol-2-yl)-2,5-diphenyltetrazolium bromide) assay (Fig. S17) under different conditions of laser power, laser heating time and nanoparticles incubation concentration. In the MTT experiment, the size of the heating laser spot is enlarged to evenly irradiate the cells of the experimental group in the 96-well plate. At this time, the laser spot size is 1 cm². The maximum heating laser power density on the surface of our sample is 0.032 mJ/cm². This laser power is slightly higher than the actual imaging conditions. And in imaging conditions, the heating laser power density is 0.029 mJ/cm² and the spot diameter is 200 μm². When changing other factors, the heating conditions use the maximum laser heating power. When changing the laser power density, the laser heating time used is 10 minutes, and the concentration of gold nanoparticles is 47.5pM. The cell survival rate was >96% under above experimental conditions. These results clearly suggested that current AMSM method has a minimized photodamage effect to cell viability.

Supplementary Note 3: Supplementary Videos

This video is a dynamic imaging of 9 nm gold nanoparticles in a HeLa cell.

REFERENCES

1. C. D. S. Brites, X. Xie, M. L. Debasu, X. Qin, R. Chen, W. Huang, J. Rocha, X. Liu and L. D. Carlos, *Nat. Nanotechnol.*, 2016, **11**, 851-856.
2. C. D. S. Brites, M. C. Fuertes, P. C. Angelomé, E. D. Martínez, P. P. Lima, G. J. A. A. Soler-Illia and L. D. Carlos, *Nano Lett.*, 2017, **17**, 4746-4752.
3. J. H. Hodak, A. Henglein and G. V. Hartland, *J. Phys. Chem. B*, 2000, **104**, 9954-9965.
4. A. Heber, M. Selmke and F. Cichos, *Phys. Chem. Chem. Phys.*, 2015, **17**, 20868-20872.
5. M. Selmke, M. Braun and F. Cichos, *ACS Nano*, 2012, **6**, 2741-2749.
6. Z. Chen, X. Shan, Y. Guan, S. Wang, J.-J. Zhu and N. Tao, *ACS Nano*, 2015, **9**, 11574-11581.
7. M. Selmke, M. Braun and F. Cichos, *Opt. Express*, 2012, **20**, 8055-8070.
8. D. Guanghua, A. D. Guido, F. Werner, G. Christoph, H. Volker, K. Reiner, K. Alexandra, T. Laura, A. F. Anna and D. Günther, *Radiation Research*, 2011, **176**, 706-715.